RESEARCH ARTICLE

Effects of Body Shadowing in LoRa Localization Systems

LUZ E. MARQUEZ[ID]**1, (Member, IEEE), ALFONSO BAHILLO2,**
MARIA CALLE[ID]**3, (Senior Member, IEEE), AND IGNACIO DE MIGUEL**[ID]**2, (Senior Member, IEEE)**
[1]Faculty of Engineering, Institución Universitaria de Barranquilla, Barranquilla 080002, Colombia
[2]Department of Signal Theory and Communications and Telematics Engineering, Universidad de Valladolid, 47011 Valladolid, Spain
[3]Department of Electrical and Electronics Engineering, Universidad del Norte, Barranquilla 080001, Colombia

Corresponding author: Luz E. Marquez (lmarquez@unibarranquilla.edu.co)

ABSTRACT Applications where a person carries environmental sensors benefit from knowing the position of the individual. Researchers can locate the device by analyzing the radio signals used for sending information. However, it is necessary to know the impact of body obstruction on communication links and, therefore, on the localization system. The paper studies this impact by using field tests employing one LoRa node with an omnidirectional antenna in an outdoor parking lot with vegetation. The tests use four LoRa gateways located in the corners of the area to measure the signals with and without body obstruction. The node was located on the subject's chest to maximize signal obstruction. Results show that signal strength decreases by an average of 3 dB on links with body shadowing. Additionally, the study uses these signals with machine learning and Kalman filter localization algorithms. Finally, the results show that body shadowing affects location accuracy in most methods. These results are useful for IoT researchers that need to locate people carrying LoRaWAN devices but cannot use GPS/GNSS due to energy constraints.

INDEX TERMS Body obstruction, environmental sensor, localization, LoRaWAN, RSSI.

I. INTRODUCTION

As part of the sustainable development goals of some governments, smart city projects are driving the growing demand for outdoor environmental quality monitoring sensors [1]. Knowing the location of wireless environmental monitoring sensors is essential for identifying, interpreting, and tracking the measured values [2]. The use of GPS (Global Positioning Systems) or GNSS (Global Navigation Satellite Systems) is common due to their accuracy and adequate outdoor performance [3]. However, using an additional module for positioning in low-power devices implies a significant increase in power consumption [4]. Wireless technologies such as LPWAN (Low Power Wide Area Network) allow

the application of localization techniques, such as triangulation, multilateration [4], and fingerprinting [5]. One of the most widely used LPWAN technologies is LoRaWAN (Long Range Wide Area Network) [6], a low-power, wide-range communications technology useful for the Internet of Things (IoT) and smart cities [7].

Portable multisensor platforms with LoRaWAN are available to support environmental monitoring with mobile nodes [8]. The portability of these nodes on the human body opens opportunities for mobile monitoring. However, this application requires determining the impact of body shadowing on the signals and the accuracy of the node location system [9].

Exposure of a human body to radio frequencies can cause attenuation in the system [10], [11]. For example, the study in [12] shows a model with obstruction of up to 6 dB for the GSM-900 band. Another paper employed Received Signal

The associate editor coordinating the review of this manuscript and approving it for publication was Mauro Fadda[ID].

Strength Indicator (RSSI) measurements showing a 13 dB difference in a Radio Frequency Identification RFID-900 system with body obstruction [13]. However, there are no studies analyzing the effect of human shadowing in LoRaWAN communications.

On the other hand, the literature regarding localization in LoRaWAN is rich, especially using RSSI values. Some works used the multilateration technique based on RSSI [14], while [15] and [16] used trilateration. A different method is fingerprinting, which has improved accuracy over lateration-based methods [17]. Several papers employed this method along with machine learning (ML) techniques for node location [18], [19], [20], [21], [22], [23], [24]. The most common techniques are K-Nearest Neighbors (KNN) [19], [20], [21], [22], [23], [24], Support Vector Regression Machine (SVR) [18], [21], [22], [24], Neural Networks [20], [23], Random Forest and other variants of Decision Trees [18], [20], [21], [22], [24]. The best performance in these works was obtained by [18] using the Smoothing Spline algorithm, with an outdoor area of 3422 m^2, static nodes, and an error of 9.4 m. The studies present noisy environments and large areas but do not evaluate the effect of body shadowing in LoRaWAN localization.

Consequently, this paper evaluates the RSSI behavior from a LoRa node, with and without the obstruction of a human body. The operating frequency of LoRa in this work is about 900MHz. At that frequency there are several works that have analyzed the shadow effect of the human body at multiple rotation angles and in free space conditions, both with measurements and in simulation (e.g. [11], [12], [13]). The studies were developed with a plane wave with vertical polarization instead of LoRa modulation. However, these works provide a basis for comparison with the present study.

Moreover, the article applies localization techniques based on RSSI to determine the effect of the body on the accuracy of these techniques. Section II presents the experimental design and results of LoRa performance, with and without human shadowing. Section III applies these results to different localization algorithms and compares their performance. To the best of the authors' knowledge, this is the first work to describe the impact of body obstruction in LoRaWAN localization systems. This work will be helpful for the research community that requires locating on-body environmental sensors.

II. LORA PERFORMANCE WITH HUMAN SHADOWING
A. EXPERIMENTAL SETUP
The test scenario was an outdoor parking lot with a 100 m × 50 m area, as shown in Fig. 1. The experimental test is an approximation to reality because LoRa is designed for long distances. However, this outdoor scenario allows an easy approach to evaluate performance with realistic obstacles such as trees, and the results should not be different placing the antennas at distances of 100 meters. Since the working frequency is around 900 MHz, the test is in the far field

(a)

(b)

FIGURE 1. (a) Satellite view where the yellow triangles identify the gateways and the blue dots indicate the node positions. (b) Trees in the test area.

region (as that zone starts below 0.5 meters); therefore, the RF signal characteristics are maintained until its disappearance. This approach of studying LoRa performance in small outdoor areas has already been used in other works like [15], [25], [26].

The experimental test locations were marked using a Trimble M3 DR3 total station; this device provides the geographic coordinates of each point with an accuracy in the order of millimeters [27]. Due to time and weather restrictions, the experiments employed 16 locations where the LoRa node transmitted to the four gateways. Fig. 1 (a) shows these test points (blue dots) over a satellite image of the site. Fig. 1 (b) illustrates the trees in the test area.

The experiments without body obstruction located the LoRa node on a tripod. Then, tests placed the node on a person's chest because this position creates the most obstruction [28]. The subject provided an informed consent.

The equipment used in the measurement campaign included four LoRaWAN RisingHF gateways [29] and a WisTrio LPWAN Tracker node, operating at 915 MHz [30]. This device worked at 5470 bps on channels 0-3 with enabled ADR (Adaptive Data Rate). However, more than 90% of the collected data uses Spreading Factor (SF) 7. Therefore, ADR activation does not significantly affect the results. Table 1

TABLE 1. Characteristics of devices.

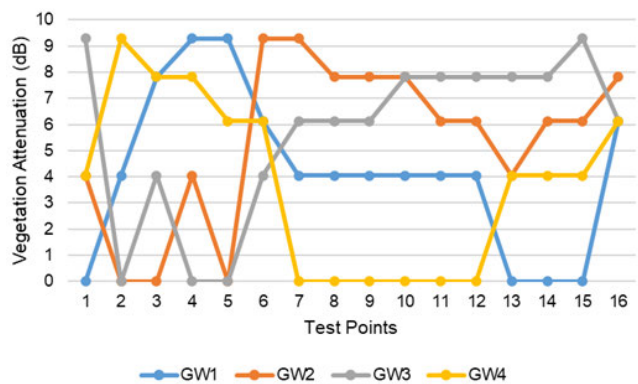| Features	Node	Gateways
Device	WisTrio LPWAN Tracker Node RAK5205	LoRaWAN RisingHF gateway
Max. Tx power	20 dBm	27 dBm
Sensitivity	-130 dBm	-142.5 dBm
Antenna	2.5 dBi SMA LoRa Antenna	0 dBi rubber duck Antenna
Antenna radiation	Omni-directional pattern	Omni-directional pattern
Height of the antennas	1.4 m	1.5 m

FIGURE 2. Attenuation caused by vegetation for each node-gateway link.

shows the characteristics of the equipment used in the experimental setup.

All devices used externally connected omnidirectional antennas; thus, we did not include their radiation pattern in the RSSI variation study.

B. VEGETATION
Trees and bushes in the work area caused attenuation. The testing scenario included semi-dense and dense vegetation. Therefore, the research incorporated the effect on the signal by using a vegetation loss model. The link attenuation depended on the depth of the foliage [31]. Equation (1) computes this loss:

$$L_{veg} = 0.2f^{0.3}d^{0.6}[dB] \qquad (1)$$

where f is the frequency (in MHz) and d is the foliage depth (m) [31].

At the test site, this attenuation changes according to vegetation density on each link, i.e., between the node location and each gateway. Fig. 2 shows the vegetation attenuation values calculated for each link using (1).

Fig. 2 shows that different node-gateway links have attenuation greater than 7 dB. Similarly, at least one node-gateway link has minimum vegetation obstruction (0 dB). Fig. 1 (a) shows that the links for test points 7 to 15 have a comparable position concerning the trees at the center of the working area. Consequently, Fig. 2 exhibits similar behavior in positions
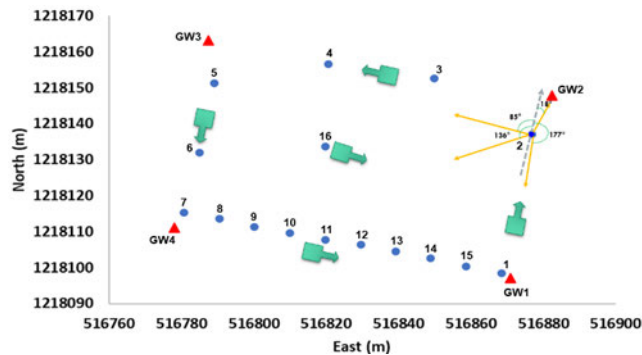

FIGURE 3. Tests with human shadowing. The red triangles are the gateways, and the blue circles are the test points. The green symbols indicate the body's position (square) and the node (arrow).

7 to 15, with variations specific to each link according to the rest of the vegetation. In fact, vegetation attenuation affects the path loss exponent and the received signal levels on each link.

C. EFFECT OF HUMAN SHADOWING
1) OBSTRUCTION TYPES
Fig. 3 shows the test points, illustrating the location of the node with body shadowing. The green symbols include a square representing the person and one arrow showing the node position. All figures show UTM coordinates, Zone 18.

According to the orientation of the node, the body generates complete obstruction (NLOS), a semi-obstruction (Quasi Line-of-Sight, QLOS), and no obstruction (LOS) for different gateways. The relative transmission angles are classified according to the ranges of (2), according to [28]:

$$LOS \rightarrow [0°, 67.5°] \cup [292.5°, 360°]$$
$$QLOS \rightarrow [67.5°, 112.5°] \cup [247.5°, 292.5°]$$
$$NLOS \rightarrow [112.5°, 247.5°] \qquad (2)$$

Fig. 3 illustrates the relative transmission angles for test point 2. In this case, the transmission angle is approximately 177° to GW1 (NLOS), 18° to GW2 (LOS), 85° to GW3 (QLOS), and 136° to GW4 (NLOS).

Fig. 4 shows the transmission angles between each test point and the gateways considering the body orientation. The behavior at positions 8 to 15 is similar due to the locations of the body concerning the different gateways.

2) EFFECTS ON RSSI
Each gateway provides information regarding RSSI levels, signal-to-noise ratio (SNR), channel frequency, and the reception time of each packet.

The information of each packet received simultaneously at the four gateways allows the creation of a radio map. This map includes the RSSI values for each test point with the corresponding geographic coordinate obtained with the Trimble. This coordinate is the ground truth for the location experiments. The measurement campaign uses more than
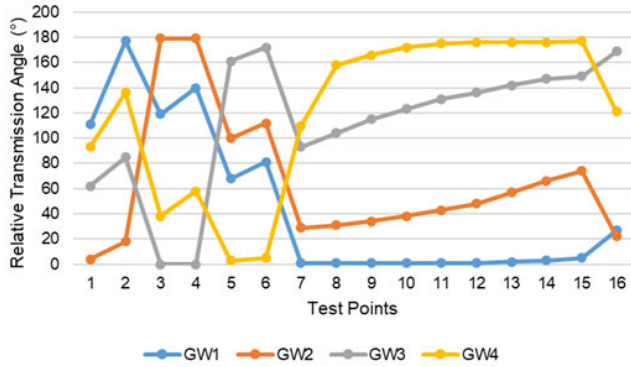
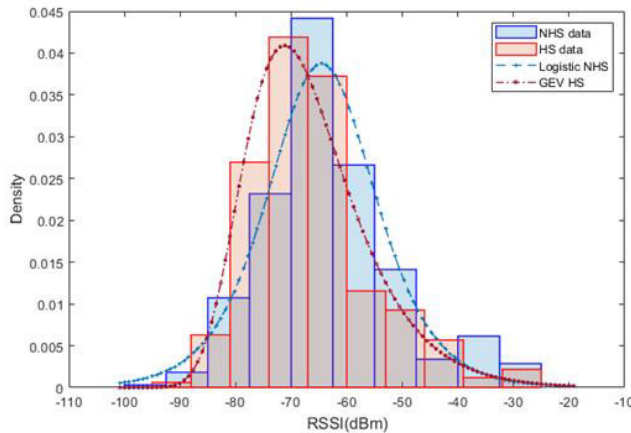**FIGURE 4.** Relative transmission angle for each node-gateway link.

FIGURE 5. RSSI histogram for tests with and without body obstruction.

FIGURE 6. RSSI values NHS (blue) and HS (orange), by Gateway 1.

FIGURE 7. RSSI values NHS (blue) and HS (orange), by Gateway 2.

FIGURE 8. RSSI values NHS (blue) and HS (orange), by Gateway 3.

FIGURE 9. RSSI values NHS (blue) and HS (orange), by Gateway 4.

50 packets per position per gateway in each case (with and without body obstruction). After the outlier elimination process, data includes 40 measurements per position for each gateway, i.e., 2560 RSSI values with body obstruction and the same number without it.

Fig. 5 shows the histograms of the data for both NHS (Non-Human-Shadowing) and HS (Human-Shadowing) scenarios. The histogram for the NHS scenario shows a distribution of RSSI levels displaced to the right compared to the HS distribution. Applying Tukey honestly significant difference (HSD) to both data sets yields a 3 dB difference with 95% confidence. Thus, RSSI levels decrease in the HS scenario. Furthermore, Fig. 5 shows the best probability distribution fit for each data set. The log-likelihood statistic and Kolmogorov-Smirnov test indicate that the best fitting distribution for the NHS data is Logistic, while for HS is Largest Extreme Value (GEV in the figure). According to these results, HS behaves as a random phenomenon whose values predominate in the lower levels.

Fig. 6 to 9 display the box-whiskers plots of RSSI measurements obtained in each gateway, without and with body obstruction. As expected, RSSI is higher when the nodes are close to the GWs. For example, according to Fig. 3 positions 1, 14 and 15 are closer to GW 1, and these positions
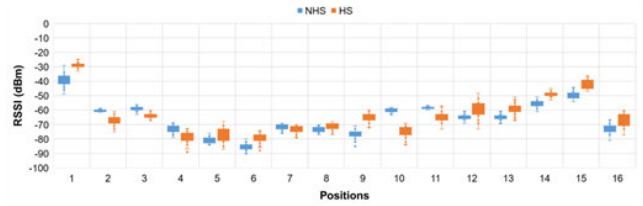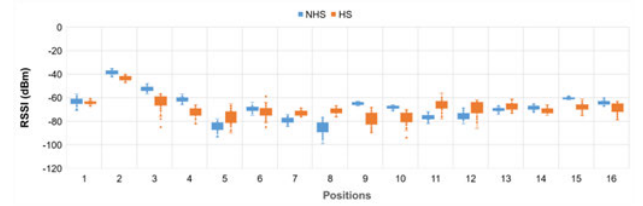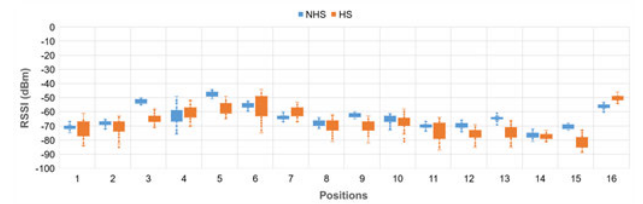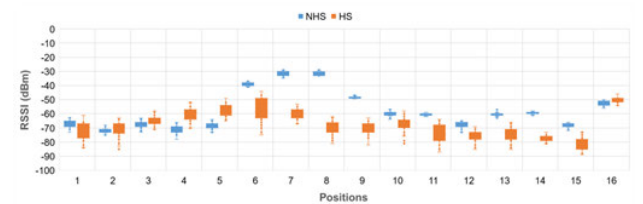
show larger RSSI levels in Fig. 6. The same behavior occurs in positions 2 and 3 for GW 2 (Fig. 7), positions 3 to 6 for GW 3 (Fig. 8) and positions 6 to 9 for GW 4 (Fig. 9). Moreover, position 16 has a large level of RSSI for GWs 3 and 4, showing a direct line of sight in these links, consistent with Fig. 1a. The values in the HS scenario (orange) tend to be smaller than NHS (blue). The results in Figs. 6 to 9 are consistent with the location and the angles shown in Figs. 3 and 4. Comparing the HS and NHS values for LOS links, the Tukey HSD method indicates no significant difference between the means. However, the statistics show differences between their standard deviations, showing the randomness of this type of testing in the given scenario. The mean values for QLOS links also show no significant difference.

Furthermore, some mean RSSI levels for HS are higher than NHS. This phenomenon results from the variability of the signal in the presence of the body. As an illustration,
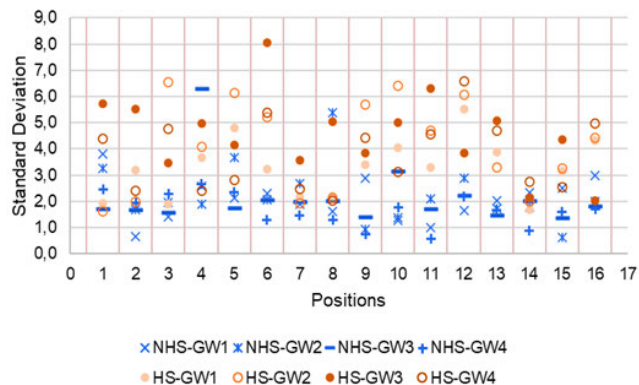
FIGURE 10. Standard deviation by position.

Fig. 10 shows the standard deviation of RSSI values by position, where the circles correspond to HS and non-circles represent NHS.

For example, Fig. 6 shows that, for position 15 at gateway 1, the average RSSI is higher with HS; however, Fig. 10 shows that gateway 1 HS also has a higher standard deviation than NHS, showing the effect of body obstruction on the signal.

Nevertheless, the behavior of the data collected illustrates a direct effect on RSSI levels due to the obstruction caused by the body to different communication links. On average, the RSSI levels with body obstruction decrease by 3 dB compared to the link without obstruction. LoRa shows smaller attenuation than that reported in [11], [12] for GSM and [13] for RFID. In those cases, the 900 MHz signal, decays by 25 dB [11], 6 dB [12] and 13 dB [13] in the presence of the body. This behavior demonstrates the robustness of LoRa modulation compared to other technologies for the same frequency band.

III. EFFECT OF HUMAN SHADOWING IN LORA LOCALIZATION

The change in RSSI may affect localization results. Hence, the research applied the measured NHS RSSI values to different localization methods and then repeated the same procedure with HS data. The methods employed are SVR, Extra Trees, KNN, MLP algorithms, and Extended Kalman Filter (EKF). The research selected these algorithms because they are widely used for localization in wireless networks [32].

A. ALGORITHM COMPARISON

This research employed 70% of data for training, 15% for validation, and 15% for testing. The data was preprocessed, modifying the representation of the sample values. There are four data representation schemes for localization, i.e., positive, normalized, exponential, and powed [20], [33], [34], [35]. We used Python for each data representation scheme and ML algorithm and Matlab for the filter-based algorithm.

TABLE 2. Hyperparameters of the ML algorithms.

Algorithm	NHS	HS
SVR	Kernel= RBF Degree =3 C=1000 Epsilon=0.05	Kernel= RBF Degree =3 C=1000 Epsilon=0.05
KNN	Representation of data: Powed β=1 Metric: Braycurtis k value = 1	Representation of data: Powed β=0.8 Metric: Braycurtis k value = 1
Extra Trees	N estimators = 180 Max depth = 19 Min samples split = 2 Representation of data: Exponential α = 15	N estimators = 100 Max depth = 19 Min samples split = 2 Representation of data: Exponential α = 20
MLP	Layers: 7 Nodes per layer: 1024, 1024, 1024,256, 256,128, 128,2 Batch normalization RELU activation function Adam optimization method L2 regularization, Dropout rate =0.15	Layers: 7 Nodes per layer: 1024, 512, 1024,256, 256,128, 128,2 Batch normalization RELU activation function Adam optimization method L2 regularization, Dropout rate =0.15

TABLE 3. Average location errors (m).

Algorithm	NHS	HS
SVR	33.80	33.80
KNN	**0.93**	**5.51**
Extra Trees	1.76	6.58
MLP	3.77	7.94
EKF	26.00	34.61

Table 2 shows the hyperparameters of each ML algorithm that obtained the best results. In the table, RBF means Radial Basis Function, C is the Regularization parameter, and RELU means Rectified Linear Activation Unit.

Table 3 presents the average errors obtained for the four ML methods developed and the Kalman filter-based algorithm. The results show that KNN presents the best performance in both scenarios (NHS and HS).

Table 3 shows that the estimation errors differ for the NHS and HS test scenarios. The average error is larger than 5 m in the HS case, whereas the NHS case has an average error of less than 4 m in three ML models. This result shows the effect on the RSS-based localization system when the LoRa device experiences human shadowing.

Additionally, Table 3 shows that three of the ML algorithms employed in this work obtained smaller errors than studies with similar areas working at 915 MHz, such as [14]. According to [14], the localization accuracy of tens of meters
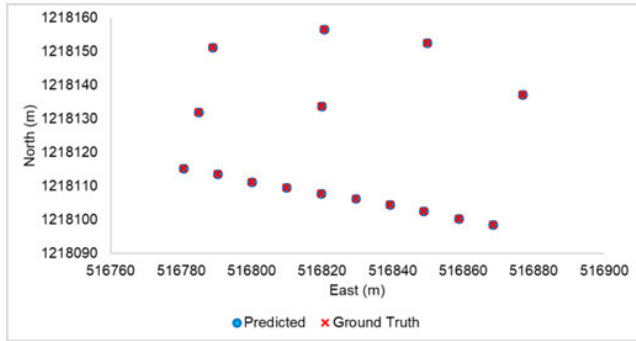
FIGURE 11. True and Predicted Locations for KNN, NHS and HS.
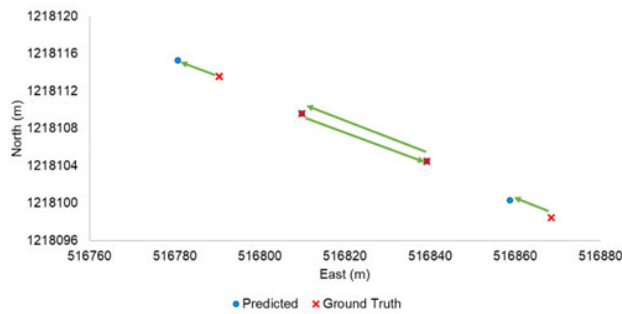

FIGURE 12. True and predicted locations, KNN, NHS scenario.

is sufficient for applications like the one proposed in this work.

The results from the Kalman filter-based algorithm display a larger localization error than those employing ML techniques.

B. ANALYSIS OF KNN AND EXTRA TREES
According to Table 3, KNN and Extra Trees obtained the best localization performance. Thus, we provide a more detailed analysis of them.

1) KNN
The KNN model predicts the coordinates for the node location. Fig. 11 shows the ground truth (red crosses) and the predicted values (blue dots) for the NHS and HS scenarios.

Fig. 11 displays a complete match between the predicted points and the true coordinates. The reason is KNN takes each sample to the nearest neighbor, whether it matches the true position or another one in the dataset. Therefore, the algorithm creates erroneous predictions that coincide with a different coordinate.

Fig. 12 and Fig. 13 show the locations that present errors in the NHS and HS scenarios, respectively. The green arrows indicate the displacement each point suffered from the ground truth and the algorithm's prediction, i.e., the position error.

Fig. 12 shows that the KNN algorithm erroneously predicted four positions in the NHS scenario, with errors of 10 and 30 m.

Fig. 13 illustrates that HS performance of the KNN algorithm is worse than NHS, as it erroneously predicted eight positions, with errors between 10 m and 50 m.
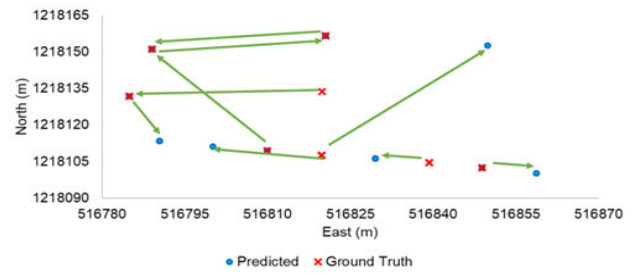

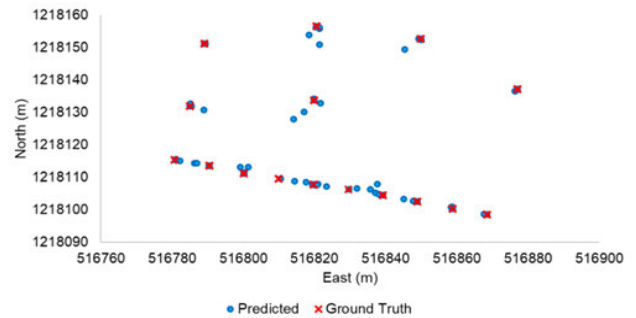**FIGURE 13.** True and predicted locations, KNN, HS scenario.

FIGURE 14. True and predicted locations, extra trees, NHS.
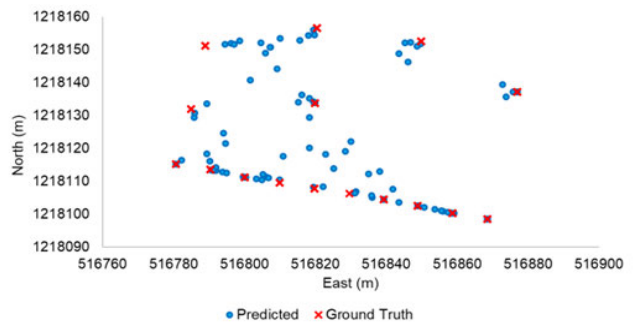

FIGURE 15. True and predicted locations, extra trees, HS.

2) EXTRA TREES
The Extra Trees algorithm predicts positions that do not precisely match the ground truth. Fig. 14 and Fig. 15 present the predicted and true locations in the Extra Trees algorithm for NHS and HS respectively. In each case, the predicted values are close to the real ones, with less variability in the NHS scenario than in HS. Fig. 14 illustrates that Extra Trees can predict the node's location with errors of the order of centimeters with a maximum of 28 m. Fig. 15 shows how the Extra Trees algorithm locates the node with errors of the order of centimeters, up to 32.5 m maximum.

IV. CONCLUSION
This paper shows that the signal in LoRaWAN systems degrades when a human body obstructs any transmission links. Results showed that the transmission angle to the gateway varies as the node changes position, along with the degree of obstruction generated by the body. Additionally, results show an average decrease of 3 dB in RSSI values with human shadowing.

Furthermore, the paper evaluates the effect of the body on LoRaWAN localization using RSSI-based methods. The results indicate that EKF exhibits larger errors than ML-based methods. The best performing algorithm was KNN, with an average error of 0.93 m for the NHS scenario and 5.51 m for HS. However, the error variability of KNN is larger than Extra Trees; hence, the latter would produce estimates with smaller individual errors than KNN. Moreover, the results show a difference close to 4 m for most ML algorithms, comparing NHS and HS scenarios. This difference demonstrates the impact of human body obstruction on the localization system. Therefore, future work requires mechanisms to mitigate the shadowing effects caused by the body in static and moving scenarios.

REFERENCES

[1] C. Toma, A. Alexandru, M. Popa, and A. Zamfiroiu, "IoT solution for smart cities' pollution monitoring and the security challenges," *Sensors*, vol. 19, no. 15, p. 3401, Aug. 2019, doi: 10.3390/s19153401.

[2] A. Khapalov, "Source localization and sensor placement in environmental monitoring," *Int. J. Appl. Math. Comput. Sci.*, vol. 20, no. 3, pp. 445–458, Sep. 2010, doi: 10.2478/v10006-010-0033-3.

[3] F. Lemic, A. Behboodi, J. Famaey, and R. Mathar, "Location-based discovery and vertical handover in heterogeneous low-power wide-area networks," *IEEE Internet Things J.*, vol. 6, no. 6, pp. 10150–10165, Dec. 2019, doi: 10.1109/JIOT.2019.2935804.

[4] I. Daramouskas, V. Kapoulas, and T. Pegiazis, "A survey of methods for location estimation on low power wide area networks," in *Proc. 10th Int. Conf. Inf., Intell., Syst. Appl. (IISA)*, Jul. 2019, pp. 1–4, doi: 10.1109/IISA.2019.8900701.

[5] J. Purohit, X. Wang, S. Mao, X. Sun, and C. Yang, "Fingerprinting-based indoor and outdoor localization with LoRa and deep learning," in *Proc. IEEE Global Commun. Conf. (GLOBECOM)*, Dec. 2020, pp. 1–6, doi: 10.1109/GLOBECOM42002.2020.9322261.

[6] Q. M. Quadir, T. A. Rashid, N. K. Al-Salihi, B. Ismael, A. A. Kist, and Z. Zhang, "Low power wide area networks: A survey of enabling technologies, applications and interoperability needs," *IEEE Access*, vol. 6, pp. 77454–77473, 2018, doi: 10.1109/ACCESS.2018.2883151.

[7] L. E. Marquez, A. Osorio, M. Calle, J. C. Velez, A. Serrano, and J. E. Candelo-Becerra, "On the use of LoRaWAN in smart cities: A study with blocking interference," *IEEE Internet Things J.*, vol. 7, no. 4, pp. 2806–2815, Apr. 2020, doi: 10.1109/JIOT.2019.2962976.

[8] A. Simo, S. Dzitac, I. Dzitac, M. Frigura-Iliasa, and F. M. Frigura-Iliasa, "Air quality assessment system based on self-driven drone and LoRaWAN network," *Comput. Commun.*, vol. 175, pp. 13–24, Jul. 2021, doi: 10.1016/j.comcom.2021.04.032.

[9] Y. Li, Y. Zhuang, X. Hu, Z. Gao, J. Hu, L. Chen, Z. He, L. Pei, K. Chen, M. Wang, X. Niu, R. Chen, J. Thompson, F. M. Ghannouchi, and N. El-Sheimy, "Toward location-enabled IoT (LE-IoT): IoT positioning techniques, error sources, and error mitigation," *IEEE Internet Things J.*, vol. 8, no. 6, pp. 4035–4062, Mar. 2021, doi: 10.1109/JIOT.2020.3019199.

[10] T. Otim, A. Bahillo, L. E. Díez, P. Lopez-Iturri, and F. Falcone, "FDTD and empirical exploration of human body and UWB radiation interaction on TOF ranging," *IEEE Antennas Wireless Propag. Lett.*, vol. 18, no. 6, pp. 1119–1123, Jun. 2019, doi: 10.1109/LAWP.2019.2910378.

[11] A. Bahillo, J. Blas, P. Fernandez, R. M. Lorenzo, S. Mazuelas, and E. J. Abril, "E-field assessment errors associated with RF dosemeters for different angles of arrival," *Radiat. Protection Dosimetry*, vol. 132, no. 1, pp. 51–56, Aug. 2008, doi: 10.1093/rpd/ncn275.

[12] A. Bahillo, J. Blas, P. Fernandez, S. Mazuelas, A. Vinuela, R. M. Lorenzo, and E. J. Abril, "E-field errors associated with RF dosimeters for RF human exposure assessment in urban environments," in *Proc. 30th Annu. Int. Conf. IEEE Eng. Med. Biol. Soc.*, Aug. 2008, pp. 2821–2824, doi: 10.1109/IEMBS.2008.4649789.

[13] A. Bahillo, J. Prieto, S. Mazuelas, R. M. Lorenzo, P. Fernandez, and E. J. Abril, "E-field assessment errors caused by the human body on localization systems," in *Proc. IEEE 71st Veh. Technol. Conf.*, 2010, pp. 1–5, doi: 10.1109/VETECS.2010.5493636.

[14] H. Kwasme and S. Ekin, "RSSI-based localization using LoRaWAN technology," *IEEE Access*, vol. 7, pp. 99856–99866, 2019, doi: 10.1109/ACCESS.2019.2929212.

[15] A. Vazquez-Rodas, F. Astudillo-Salinas, C. Sanchez, B. Arpi, and L. I. Minchala, "Experimental evaluation of RSSI-based positioning system with low-cost LoRa devices," *Ad Hoc Netw.*, vol. 105, Aug. 2020, Art. no. 102168, doi: 10.1016/j.adhoc.2020.102168.

[16] P. Manzoni, C. T. Calafate, J.-C. Cano, and E. Hernández-Orallo, "Indoor vehicles geolocalization using LoRaWAN," *Future Internet*, vol. 11, no. 6, p. 124, May 2019, doi: 10.3390/fi11060124.

[17] C. Laoudias, A. Moreira, S. Kim, S. Lee, L. Wirola, and C. Fischione, "A survey of enabling technologies for network localization, tracking, and navigation," *IEEE Commun. Surveys Tuts.*, vol. 20, no. 4, pp. 3607–3644, 4th Quart., 2018, doi: 10.1109/COMST.2018.2855063.

[18] M. Anjum, M. A. Khan, S. A. Hassan, A. Mahmood, H. K. Qureshi, and M. Gidlund, "RSSI fingerprinting-based localization using machine learning in LoRa networks," *IEEE Internet Things Mag.*, vol. 3, no. 4, pp. 53–59, Dec. 2020, doi: 10.1109/IOTM.0001.2000019.

[19] M. Aernouts, R. Berkvens, K. Van Vlaenderen, and M. Weyn, "Sigfox and LoRaWAN datasets for fingerprint localization in large urban and rural areas," *Data*, vol. 3, no. 2, p. 13, Apr. 2018, doi: 10.3390/data3020013.

[20] G. G. Anagnostopoulos and A. Kalousis, "A reproducible comparison of RSSI fingerprinting localization methods using LoRaWAN," in *Proc. 16th Workshop Positioning, Navigat. Commun. (WPNC)*, Oct. 2019, pp. 1–6, doi: 10.1109/WPNC47567.2019.8970177.

[21] T. Janssen, R. Berkvens, and M. Weyn, "Comparing machine learning algorithms for RSS-based localization in LPWAN," in *Proc. Int. Conf. P2P, Parallel, Grid, Cloud Internet Comput.*, in Lecture Notes in Networks and Systems, 2020, pp. 726–735, doi: 10.1007/978-3-030-33509-0_68.

[22] T. Janssen, R. Berkvens, and M. Weyn, "Benchmarking RSS-based localization algorithms with LoRaWAN," *Internet Things*, vol. 11, Sep. 2020, Art. no. 100235, doi: 10.1016/j.iot.2020.100235.

[23] I. Daramouskas, V. Kapoulas, and M. Paraskevas, "Using neural networks for RSSI location estimation in LoRa networks," in *Proc. 10th Int. Conf. Inf., Intell., Syst. Appl. (IISA)*, Jul. 2019, pp. 1–7, doi: 10.1109/IISA.2019.8900693.

[24] F. Lemic, V. Handziski, M. Aernouts, T. Janssen, R. Berkvens, A. Wolisz, and J. Famaey, "Regression-based estimation of individual errors in fingerprinting localization," *IEEE Access*, vol. 7, pp. 33652–33664, 2019, doi: 10.1109/ACCESS.2019.2903880.

[25] E. Svertoka, A. Rusu-Casandra, R. Burget, I. Marghescu, J. Hosek, and A. Ometov, "LoRaWAN: Lost for localization?" *IEEE Sensors J.*, vol. 22, no. 23, pp. 23307–23319, Dec. 2022, doi: 10.1109/JSEN.2022.3212319.

[26] G. M. Bianco, R. Giuliano, F. Mazzenga, and G. Marrocco, "Multi-slope path loss and position estimation with grid search and experimental results," *IEEE Trans. Signal Inf. Process. Netw.*, vol. 7, pp. 551–561, 2021, doi: 10.1109/TSIPN.2021.3106693.

[27] Nikon-Trimble. (Oct. 2005). *USER GUIDE Trimble M3 Total Station*. Accessed: Mar. 16, 2022. [Online]. Available: http://www.geosamudra.com/datasheet/Trimble_M3_UserGuide_100A_English.pdf

[28] T. Otim, A. Bahillo, L. E. Díez, P. Lopez-Iturri, and F. Falcone, "Impact of body wearable sensor positions on UWB ranging," *IEEE Sensors J.*, vol. 19, no. 23, pp. 11449–11457, Dec. 2019, doi: 10.1109/JSEN.2019.2935634.

[29] Seeed Studio. *LoRa/LoRaWAN Gateway Kit—Seeed Wiki*. Accessed: Dec. 9, 2021. [Online]. Available: https://wiki.seeedstudio.com/LoRa_LoRaWan_Gateway_Kit/

[30] RAKwireless Technology Limited. *RAK7205/RAK5205 WisTrio LPWAN Tracker | RAKwireless Documentation Center*. Accessed: Dec. 9, 2021. [Online]. Available: https://docs.rakwireless.com/Product-Categories/WisTrio/RAK7205-5205/Overview/#product-features

[31] H. Lehpamer, *Microwave Transmission Networks: Planning, Design, and Deployment*, vol. 1. New York, NY, USA: McGraw-Hill, 2004.

[32] I. Ullah, S. Qian, Z. Deng, and J.-H. Lee, "Extended Kalman filter-based localization algorithm by edge computing in wireless sensor networks," *Digit. Commun. Netw.*, vol. 7 no. 2, pp. 187–195, May 2021, doi: 10.1016/J.DCAN.2020.08.002.

[33] G. G. Anagnostopoulos and A. Kalousis, "A reproducible analysis of RSSI fingerprinting for outdoor localization using sigfox: Preprocessing and hyperparameter tuning," in *Proc. Int. Conf. Indoor Positioning Indoor Navigat. (IPIN)*, Sep. 2019, pp. 1–8, doi: 10.1109/IPIN.2019.8911792.

[34] T. Janssen, M. Aernouts, R. Berkvens, and M. Weyn, "Outdoor fingerprinting localization using sigfox," in *Proc. Int. Conf. Indoor Positioning Indoor Navigat. (IPIN)*, Sep. 2018, pp. 1–6, doi: 10.1109/IPIN.2018.8533826.

[35] J. Torres-Sospedra, R. Montoliu, S. Trilles, Ó. Belmonte, and J. Huerta, "Comprehensive analysis of distance and similarity measures for Wi-Fi fingerprinting indoor positioning systems," *Expert Syst. Appl.*, vol. 42, no. 23, pp. 9263–9278, Dec. 2015, doi: 10.1016/j.eswa.2015.08.013.

LUZ E. MARQUEZ (Member, IEEE) received the degree in electronics engineering from the Universidad Autónoma de Colombia, Barranquilla, Colombia, in 2004, and the M.S. degree in telematics and telecommunications from the Universidad del Norte, Barranquilla, in 2014, where she is currently pursuing the Ph.D. degree in electrical and electronics engineering. She is also an Assistant Professor with the Institución Universitaria de Barranquilla, Barranquilla. Her research interests include telematics applications and communication technologies for wireless sensor networks.

ALFONSO BAHILLO received the degree and Ph.D. degrees in telecommunications engineering from the University of Valladolid, Spain, in 2006 and 2010, respectively, and the PMP Certification from PMI, in 2014. From 2006 to 2010, he was a Research Engineer with CEDETEL. From 2006 to 2011, he was an Assistant Professor at the University of Valladolid. From 2010 to 2012, he was a Product Owner with LUCE Innovative Technologies. From 2013 to 2017, he held a post-doctoral position and was the Project Manager of DeustoTech-Fundacion Deusto, Bilbao, where he trains Ph.D. students and collaborates in several national and international research projects. From 2017 to 2020, he was the Director of DeustoTech-Fundacion Deusto, University of Deusto. He has worked (leading some of them) in more than 25 regional, national, and international research projects and contracts. He has coauthored more than 35 research papers, published in international journals, published more than 40 communications in international conferences, and three national patents. His research interests include local and global positioning techniques, ambient assisted living, intelligent transport systems, wireless networking, and smart cities.

MARIA CALLE (Senior Member, IEEE) received the B.S. degree in electronics engineering from Universidad Pontificia Bolivariana, Medellín, Colombia, in 1995, and the master's degree in telecommunications and the Ph.D. degree in information sciences from the University of Pittsburgh, Pittsburgh, PA, USA, in 2006 and 2009, respectively.

She is currently a Professor with the Universidad del Norte, Barranquilla, Colombia, a Senior Researcher with Minciencias, Bogota, Colombia, and the Coordinator with the Telecommunications and Signals Research Group, Universidad del Norte. Her current research interests include low-power wide area networks, communication protocols for the Internet of Things, and engineering education.

IGNACIO DE MIGUEL (Senior Member, IEEE) received the degree and Ph.D. degrees in telecommunication engineering from the Universidad de Valladolid (UVa), Spain, in 1997 and 2002, respectively. He is currently an Associate Professor with UVa and the Coordinator of the master's degree in telecommunication engineering. He has also been a Visiting Research Fellow at University College London, U.K. His research interests include design, control and performance evaluation of communication infrastructures, edge computing, and the application of artificial intelligence techniques in those environments. He has been a member of the TPC of several international conferences, besides being the Chair of the TPC and the Local Organizing Committee of NOC, in 2009. He was a recipient of the Nortel Networks Prize for the Best Ph.D. Thesis on Optical Internet, in 2002, awarded by the Spanish Institute and the Association of Telecommunication Engineers (COIT/AEIT).

• • •